Model Validation: Comparing PlaSim-LSG Model Climatology against ERA5 Reanalysis Data

Arianna Magagna
arianna.magagna@studio.unibo.it

Department of Physics
Science of Climate

This study evaluates the performance of the coupled PlaSim–LSG Earth System Model of Intermediate Complexity (EMIC) by comparing its climatology with observational data from the ERA5 reanalysis dataset. The model combines the Planet Simulator (PlaSim) and the Large-Scale Geostrophic (LSG) ocean model to simulate interactive atmosphere–ocean dynamics efficiently over long timescales. Validation is performed using an ensemble of 100 long-term simulations under a fixed atmospheric CO concentration (354 ppm), approximating the effective radiative forcing of the 2005–2015 period. Key atmospheric and oceanic variables—such as sea surface temperature, 850 hPa air temperature, sea level pressure, zonal wind speed, and sea ice cover—are compared with ERA5 using metrics including mean bias error, root mean square error, and spatial correlation. Results show good agreement in most regions but highlight a persistent warm bias and weak circulation in the Southern Ocean, likely linked to coarse resolution and simplified parameterizations. Despite these limitations, the PlaSim-LSG T21 configuration is deemed suitable for studies focusing on large-scale variability, particularly in the North Atlantic, offering a practical balance between physical realism and computational cost.

Keywords: PlaSim, LSG, EMIC, climate modeling, ERA5, model validation, ocean–atmosphere coupling, Southern Ocean bias.

1 Introduction

Climate models range from highly simplified conceptual models, where components of the Earth system are represented independently, to comprehensive Earth System Models (ESMs) that include a detailed and fully coupled representation of atmospheric, oceanic, biological and geochemical processes. While this evolution has led to a more realistic simulation of Earth system processes, it has also significantly increased the computational cost. As a result, fully coupled models, despite their accuracy, often become impractical for long-term simulations or for studies that require large ensembles. On the other end of the spectrum, simplified conceptual models offer computational efficiency but lack many of the critical processes and feedbacks that are crucial in the real climate system [1, 2].

To bridge this gap, Earth-System Models of Intermediate Complexity (EMICs) were developed starting in the 1980s. EMICs capture the essential dynamics and interactions of the climate system but do so in a reduced, more computationally efficient form compared to full-scale ESMs. This makes it possible to run long-term simulations and explore wide parameter spaces or poorly understood processes using relatively modest computational resources. For this reason, EMICs are particularly useful in areas where observational or theoretical knowledge is limited. In such contexts, using an EMIC allows for a more targeted investigation of the key mechanisms, rather than attempting to replicate every detail of the system. By isolating the main drivers of the climate system, EMICs can offer a deeper insight, even if some feedbacks are represented in a simplified or approximate manner [2].

In this study, we use the coupled PlaSim–LSG model, an EMIC that combines two components: the Planet Simulator (PlaSim) and the Large-Scale Geostrophic (LSG) ocean model. The PlaSim–LSG simulates the key interactions between atmosphere, ocean and sea ice. Although it does not aim to match the resolution or complexity of full ESMs, it offers a balanced compromise: a physically grounded framework that is computationally light, while maintaining a level of model complexity sufficient to capture the essential dynamics of atmosphere–ocean coupling [3].

Version 1.18, July 13, 2025

2 PlaSim

The Planet Simulator (PlaSim) is an EMIC developed by the Meteorological Insitute of the University of Hamburg to support numerical experiments for understanding the dynamics of the climate of the Earth and Earth-like planets and moons of the solar system [3, 4]. PlaSim has been built to offer a simplified virtual laboratory to study the fundamental dynamical and thermodynamical issues, to identify feedbacks responsible for the long-term stability of the climate and to explore the causes of sudden losses of stability or abrupt change, like the impact of a volcanic eruption or the consequences of a thermohaline circulation breakdown [4]. For example, it has been used to explore past conditions of the Earth such as the snowball Earth [5] or the Permian climate [6], to analyze specific processes of the climate system using an Aquaplanet configuration [7], to investigate the Earth's global energy budget [8] or exoplanets [9].

2.1 Dynamical Core. The dynamical core of PlaSim consists of a set of differential equations that represent the fundamental laws governing large-scale atmospheric dynamics [10]. These include the conservation of momentum and mass, the first law of thermodynamics and the equation of state, simplified by the hydrostatic approximation. This formulation, which is adapted from the Portable University Model of the Atmosphere (PUMA), contains the so-called moist primitive equations in a dimensionless form, enhancing numerical stability and allowing generalization across different planetary settings [10]. The dynamical core is responsible for the evolution of the model's core prognostic variables (such as wind, temperature, pressure and humidity) based only on dynamics and thermodynamics. It operates independently from the model's physical parameterizations, which are applied

subsequently to account for unresolved subgrid-scale processes.

The dynamical equations in PlaSim are solved numerically using a combination of spectral and grid-point techniques. In the vertical, the model employs a terrain following σ-coordinate system, where σ is defined as the pressure normalized by surface pressure ($\sigma = p/p_s$). This allows the model to follow topographic variations while maintaining a consistent pressure based layering. The horizontal discretization relies on the spectral transform method, in which fields are represented by spherical harmonics for efficient calculation of derivatives [11, 12]. Vertical derivatives are computed using finite differences, with variables such as vertical velocity defined on staggered levels between the main layers to improve numerical stability. Time integration is performed using a leap-frog semi-implicit scheme [13, 14], which allows for longer time steps by treating fast waves implicitly. To suppress numerical noise associated with the leap-frog method, a Robert–Asselin time filter is applied [15, 16].

Standard horizontal spectral resolutions include T21 and T42 (approximately 5.6° and 2.8° resolution), with typical vertical resolution of 10 layers reaching up to 40 hPa. Time steps of 45 minutes (T21) and 30 minutes (T42) are used in typical configurations.

2.2 Parametrization and subsystems. In PlaSim, the effects of subgrid-scale processes that cannot be explicitly resolved by the dynamical core are represented through simplified yet physically motivated parameterizations. These include treatments for turbulent boundary layer fluxes, vertical and horizontal diffusion, radiation, moist processes, convection and cloud formation [3, 17].

Boundary Layer and Diffusion. Surface fluxes of momentum, sensible heat and latent heat are computed using bulk aerodynamic formulas based on Monin–Obukhov similarity theory, following the formulations developed for the ECHAM-3 model [18, 19]. Vertical diffusion is applied to wind, temperature and humidity using a mixing-length approach, while horizontal diffusion is calculated in spectral space.

Radiation. Radiative processes are handled using a two-stream approximation: shortwave radiation accounts for Rayleigh scattering and gaseous absorption following Lacis and Hansen (1974) [20], while longwave radiation relies on a broadband emissivity method following Sasamori (1968) [21]. Cloud radiative effects are either prescribed or parameterized using cloud properties such as albedo and emissivity, with distinctions made between high-, middle- and low-level clouds [22].

Moist processes, clouds and dry convection. Moist processes include a Kuo-type convection scheme [23, 24] and large-scale condensation is triggered when air becomes supersaturated, resulting in immediate precipitation without cloud water storage. Cloud cover is diagnosed based on relative humidity and convective precipitation rates [25]. A simple diagnostic treatment distinguishes between rainfall and snowfall based on surface temperature, so that if the temperature of the lowest level is above the freezing point (set to 271.25 K), convective and large scale precipitation is assumed to be rain, otherwise interpreted as snow. Dry convective adjustment is performed to restore dry adiabatic stability, conserving column-integrated sensible heat and fully mixing moisture in the affected layers.

Land surface and soil. The land surface scheme includes a multilayer soil model with prognostic temperatures for six layers down to 12.6 meters depth, a bucket model for soil moisture and snow storage and a river routing scheme based on linear advection [26]. Surface characteristics such as albedo, roughness length and vegetation cover are prescribed or diagnosed using an optional biome model. Glaciers are treated as land points with ice-like properties.

Ocean and sea ice. Oceanic conditions can be prescribed using sea surface temperatures and ice cover, or simulated with a slab ocean model coupled to a thermodynamic sea ice model. This model assumes a linear temperature gradient in the ice and prevents ice from storing heat: this means that sea ice is formed if the ocean temperature drops below the freezing point and is melted if the ocean temperature exceeds that value [3]. PlaSim includes a simple mixed layer (ML) ocean scheme, but coupling to a dynamic ocean model, such as LSG, is also possible for more comprehensive climate simulations, which is the case for this thesis.

3 LSG

The Large-Scale Geostrophic ocean circulation model [27, 28] is a three-dimensional grid-based model developed for long-term climate simulations. It solves a simplified form of the primitive equations, including momentum, continuity and thermodynamic equations for temperature and salinity. The model is designed for large-scale processes, where characteristic spatial scales exceed the internal Rossby radius of deformation and temporal scales are much longer than the periods of barotropic and gravity wave modes [29]. As a result, nonlinear advection terms in the momentum equations are neglected and both the hydrostatic and Boussinesq approximations are applied. Vertical friction is also ignored. Subgrid-scale mixing processes are parameterized with a depth-dependent vertical diffusion coefficient [1, 30].

The model is integrated using an implicit time integration scheme, allowing for long time steps of up to 10 days. Horizontally, the model uses a semi-staggered E-grid [31] with two $5° \times 5°$ grids offset, resulting in an effective resolution of approximately 3.5°, while the vertical dimension consists of 22 layers extending to a maximum ocean depth of 6000 meters. Scalar variables such as temperature, salinity, pressure and vertical velocity are defined at scalar points, while vector variables such as horizontal velocity components and wind stress are defined at vector points. The model initialization relies on observational data, typically from the Levitus98 dataset, providing gridded temperature and salinity fields.

4 Coupling the PlaSim Model with the LSG Ocean Model

PlaSim and LSG ocean model are coupled through the exchange of surface fluxes of momentum, heat and freshwater [1]. This coupling system guarantees a physically consistent interaction between atmosphere and ocean, maintaining the global conservation of energy and water [4, 32]. Interpolation routines adjusts the different horizontal grid structures of the two models, so that fluxes can be accurately mapped between the atmospheric and oceanic domains.

The coupling is implemented through the ML slab ocean scheme of PlaSim and the uppermost layer of the LSG ocean. Both layers are assigned a fixed depth of 50 meters:

$$\Delta z_{\mathrm{ML}}^{\mathrm{Pla}} = \Delta z_{\mathrm{UL}}^{\mathrm{LSG}} = 50\,\mathrm{m}, \tag{1}$$

where $\Delta z_{\mathrm{ML}}^{\mathrm{Pla}}$ is the depth of the PlaSim mixed layer and $\Delta z_{\mathrm{UL}}^{\mathrm{LSG}}$ is the depth of the LSG upper layer. The free surface elevation of LSG ζ, which can vary due to dynamic ocean processes, is generally small (about 1% of the upper-layer thickness) and is therefore neglected in the energy exchange calculations.

At the beginning of each LSG time step ($\Delta t_{\mathrm{LSG}} = 10$ days), the mean ML temperature simulated by PlaSim over the same interval is imposed as the temperature of the upper ocean layer in LSG. Mathematically, this is expressed as:

$$T_{\mathrm{UL}}^{\mathrm{LSG}} = T_{\mathrm{ML}}^{\mathrm{Pla}} = \frac{1}{\Delta t_{\mathrm{LSG}}} \int_{\Delta t_{\mathrm{LSG}}} T_{\mathrm{ML}}^{\mathrm{Pla}}\, dt_{\mathrm{Pla}} \tag{2}$$

After receiving the mixed-layer temperature, the LSG model performs a full ocean time step, simulating the redistribution of heat through advective processes (advection and horizontal diffusion), vertical transport (including vertical diffusion and convective adjustment) and mixing. The updated upper-layer temperature from LSG then determines the oceanic heat flux that is passed back to PlaSim for the next coupling interval.

To ensure strict energy conservation and to account for minor discrepancies between the layer depths of the two models, Equation 2 is further adjusted [32]. These corrections are necessary to close the surface energy budget and maintain consistency in long-term integrations.

Sea ice in the coupled system is simulated exclusively by the PlaSim ML module and it is prescribed in the LSG ocean model. However, over long integration periods (hundreds of years), unconstrained sea ice growth can occur at isolated grid points, particularly in the Southern Ocean. To prevent unrealistic increases in salinity of adjacent open water layers (due to excessive sea ice formation), the sea ice thickness in LSG is limited to a maximum of 9 meters.

Wind stress and freshwater fluxes (including precipitation, evaporation and runoff) are also transferred from PlaSim to LSG. These fluxes are temporally averaged over the 10-day coupling interval to smooth short-term atmospheric variability. In addition, a constant annual mean freshwater flux correction is applied to compensate for long-term water balance drift.

This coupling scheme allows PlaSim and LSG to simulate interactive atmosphere-ocean dynamics across timescales ranging from seasonal variability to millennial-scale climate equilibria, making the system particularly suitable for long-term simulations.

4.1 Parameter Settings. Following Mehling (2023) [33] and Angeloni (2020) [34], the coupled PlaSim-LSG model is configured at a horizontal spectral resolution of T21 with 10 vertical atmospheric levels, while the ocean component operates on a 3.5° horizontal grid with 22 vertical levels. Since the aim of this work is to analyze whether atmospheric internal variability only can lead to an AMOC weakening, i.e. without accounting for external forcings, the atmospheric CO_2 concentration is kept constant at 354 ppm throughout the simulations. The model is set with the standard parameterizations, except for the horizontal diffusion coefficient in the ocean, which has been adjusted according to the tuning proposed by Angeloni (2022) [1]. This adjustment specifically concerns the vertical profile of the oceanic diapycnal diffusivity A_v, which is known to strongly influence the AMOC strength and stability. In the configuration used here, the vertical diffusivity varies between 0.45×10^{-4} $\mathrm{m^2 s^{-1}}$ near the surface and 1.3×10^{-4} $\mathrm{m^2 s^{-1}}$ near the ocean bottom, following the reference setup established by Angeloni. This parameter tuning ensures a more realistic representation of ocean mixing processes, which is critical for the climate dynamics studied in this work.

4.2 Model Validation. To evaluate the realism of the model used in this work, selected variables of interest were compared against reanalysis data from years that match the simulated climate. With respect to this, it is important to note that the model simulations were conducted with a fixed atmospheric CO_2 concentration of 354 ppm, which approximately corresponds to the climate conditions during the period 2005–2015. In fact, although this CO_2 concentration closely matches the 1990 level (354.05 ppm) and it is significantly lower than the value recorded in 2010 (388.75 ppm) [35], the choice of such reference period accounts for the transient nature of the Earth's climate system. The ongoing increase in CO_2 results in a persistent radiative imbalance, currently around 0.5 $\mathrm{Wm^{-2}}$, at the surface and the top of the atmosphere [1]. If CO_2 levels were to stabilize, the Earth would continue to warm until reaching a new equilibrium, characterized by increased outgoing longwave radiation and a net zero energy imbalance.

As a result, using the 1990 CO_2 level in long-term simulations would produce a global mean temperature higher than what was observed in that year. To account for this lag between radiative forcing and temperature response, the lower fixed CO_2 concentration used in the model is interpreted in terms of an effective CO_2 period, determined with the relationship between CO_2 levels and radiative forcing, as defined in [36]:

$$\Delta F = \alpha \ln\left(\frac{\mathrm{CO_2}}{\mathrm{CO_{2ref}}}\right). \tag{3}$$

Here, the constant α is the radiative forcing coefficient, which is taken as $\alpha = 5.35$ $\mathrm{Wm^{-2}}$ following Myhre et al. [37], ΔF represents the change in radiative forcing, $\mathrm{CO_{2ref}}$ is the CO_2 concentration during the reference period, and $\mathrm{CO_2}$ is the effective concentration used in the model. By referencing the period 2005–2015, the corresponding CO_2 concentration is estimated to be approximately 354 ppm. This, indeed, is the value adopted in the simulations.

Figure 1 shows spatial differences between model output and reanalysis data for a) sea surface temperature, b) air temperature at 850 hPa, c) air pressure at sea level, d) zonal wind speed at 850 hPa and e) sea ice cover of PlaSim-LSG against ERA5 Reanalysis dataset, as summarized in Table 1. Alongside spatial maps and bias distribution, quantitative measures of model fidelity were calculated using three standard metrics:

(1) Mean Bias Error (MBE): this is defined as the average difference between the model output and the corresponding reanalysis values over the spatial domain:

$$\mathrm{MBE} = \frac{1}{N}\sum_{i=1}^{N}(M_i - R_i),$$

where M_i and R_i are the model and reanalysis values at gridpoint i respectively and N is the number of valid grid points. Bias quantifies systematic overestimation (positive bias) or underestimation (negative bias) by the model.

(2) Root Mean Square Error (RMSE): RMSE provides a measure of the magnitude of overall differences between the model and the reanalysis, giving more weight to larger errors:

$$\mathrm{RMSE} = \sqrt{\frac{1}{N}\sum_{i=1}^{N}(M_i - R_i)^2}.$$

RMSE is sensitive to large deviations and reflects both systematic and random errors.

(3) Pattern Correlation (Pearson's correlation coefficient r): this metric assesses the degree to which the spatial patterns in the model and reanalysis fields are linearly related:

$$r = \frac{\sum_{i=1}^{N}(M_i - \bar{M})(R_i - \bar{R})}{\sqrt{\sum_{i=1}^{N}(M_i - \bar{M})^2}\sqrt{\sum_{i=1}^{N}(R_i - \bar{R})^2}},$$

where $\bar{M}$ and $\bar{R}$ are the spatial means of the model and reanalysis fields, respectively. A value of $r = 1$ indicates perfect spatial agreement, while $r = 0$ implies no linear relationship.

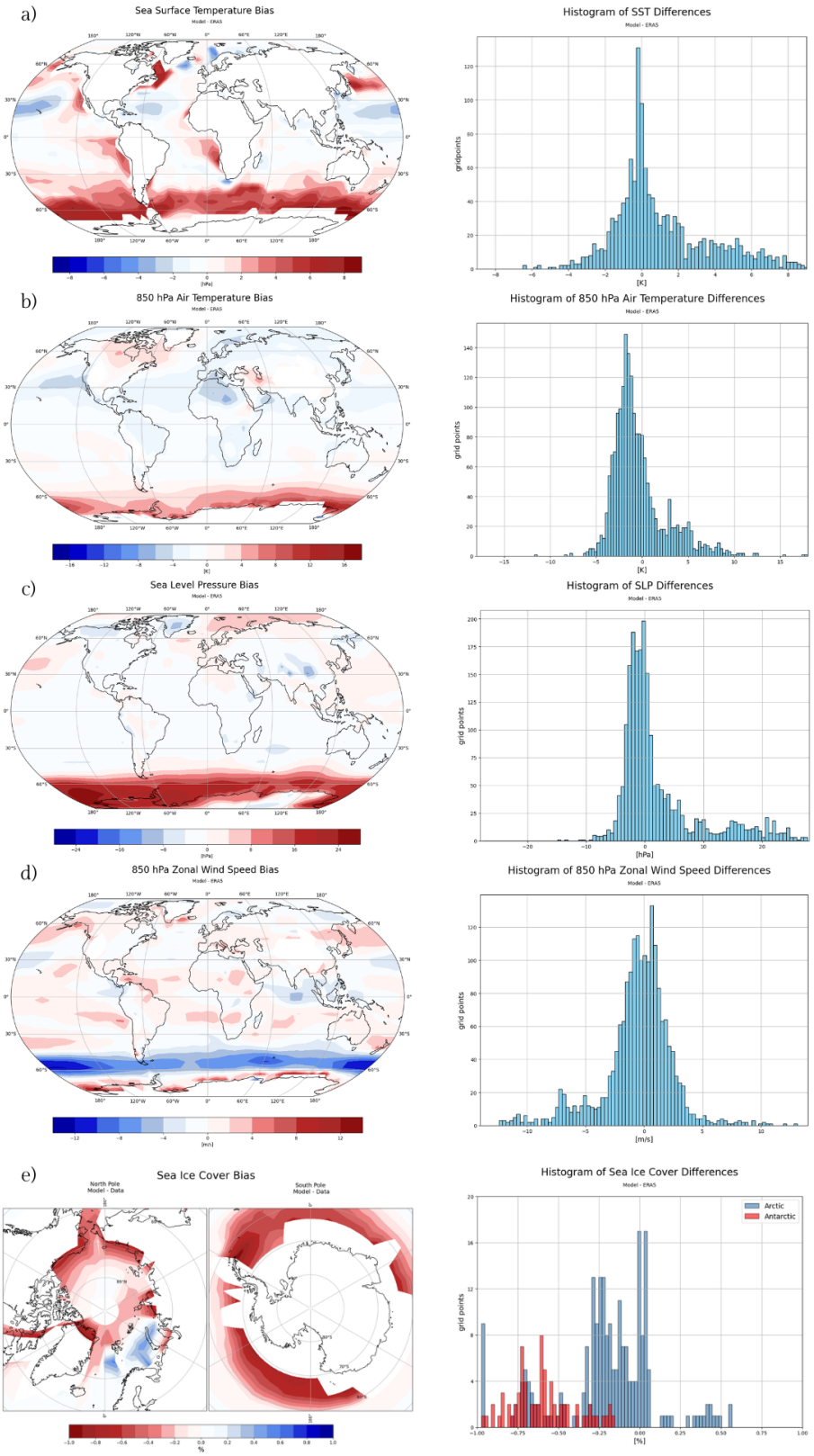

Fig. 1 Differences between simulated and observed climatologies for key variables: a) Sea Surface Temperature (SST), b) 850 hPa Air Temperature, c) Sea Level Pressure (SLP), d) 850 hPa Zonal Wind Speed, and e) Sea Ice Cover. The left column displays spatial distributions of the climatological bias (model minus observations), while the right column presents histograms of these differences across all grid points.

Variable	Domain	MBE	RMSE	r
Sea Surface Temperature	Ocean	+1.04 K	2.82 K	0.98
Temperature 850 hPa	Atmosphere	-0.38 K	3.01 K	0.97
Air Pressure at Sea Level	Atmosphere	+2.52 hPa	7.33 hPa	0.72
Zonal Wind Speed 850 hPa	Atmosphere	-0.57 m/s	3.11 m/s	0.83
Sea Ice Cover (Arctic)	Ice	-0.20%	0.36%	0.61
Sea Ice Cover (Antarctic)	Ice	-0.60%	0.63%	0.46

Table 1 Statistical comparison between PlaSim-LSG model output and reanalysis data.

All metrics were calculated over the common model domain, excluding masked or undefined grid points.

Model climatology was obtained as the average over the last 15 years of a long-term perennial simulation, using an ensemble of 100 trajectories. These results were compared to climatologies derived from ERA5 monthly averaged data on single levels for the period 2005–2015. To ensure a consistent comparison, reanalysis fields were spatially interpolated to the model's horizontal resolution (T21, 32×64 grid points) and the land-sea mask was adjusted to match that of the model.

With reference to Figure 1a, we can see an evident warm bias in the sea surface temperature climatology in the Southern Ocean, reaching up to 9 K difference in some areas. High bias regions can also be seen on most continental coasts. The bias histogram is approximately gaussian centered around 0 K, but slightly skewed to the right, confirming a general tendency toward overestimation of SSTs. A similar pattern is observed in air temperature anomalies at 850 hPa (Figure 1b), where the positive bias in the Southern Ocean reaches up to 18 K. Northern Hemisphere mid-latitudes show some cold bias areas. The histogram is sharply peaked about -2 K and is mostly symmetric, but with a noticeable warm tail. A pronounced positive sea level pressure bias is concentrated in the Southern Hemisphere, particularly around Antarctica (Figure 1c). The histogram is skewed right, showing a general overestimation of SLP. Consistently with this, a distinct negative zonal wind speed bias is found in the Southern Hemisphere, particularly over the circumpolar belt (Figure 1d). This corresponds to an underestimation of the westerly jet, which may be dynamically related to sea ice and temperature errors in the region. The histogram is slightly skewed to the left, indicating a general underestimation of zonal wind speeds. Finally, sea ice cover is strongly underestimated in both hemisphere but is slightly overestimated in some areas of the Arctic (Figure 1e). These discrepancies are once again particularly marked in the Southern Ocean, where the model fails to reproduce observed sea ice extent, consistently with the temperature bias described earlier. The histogram confirms this asymmetry, with Antarctic biases (in red) shifted significantly leftward, representing underestimation, while Arctic biases (in blue) show more dispersion.

5 Conclusions

Overall, the PlaSim-LSG T21 model has quite a good agreement with the observed values almost everywhere except for the latitudinal band between 40°S and 90°S, where all the variables analyzed show a pronounced bias. Together, these errors suggest a systematic weakening of the Southern Hemisphere circulation, likely linked to insufficient oceanic vertical mixing, coarse spatial resolution and missing processes such as cloud microphysics or eddy-driven momentum transport [1]. Efforts have been made to adjust these discrepancies. However, since the dynamics in PlaSim-LSG is completely described by the equations, it is difficult to make changes that only affect a particular region. Nevertheless, as some components of the Earth system are only present in such regions, attempts have been made on specific parameters associated to such components. Angeloni (2022) [1] explored the role of some atmospheric and oceanic model parameters that have a particular importance in the Southern Ocean, among which the oceanic vertical diffusion coefficient (correction that was indeed implemented in the simulations used for this work, included the ones used for validation), oceanic horizontal diffusion coefficient, sea ice albedo parameter and cloud albedo parameter. Besides the vertical diffusion coefficient, which did improve the previous results, all other analyses did not lead to an improvement in the southern bias. Some problems could be attributed to the coarse resolution of the model, but on the other hand using a finer resolution (as the available T42 in PlaSim) might lead to a worse description of interannual variability, which makes the coarser T21 more appropriate for some cases. In more complex models the warm bias in the Southern Ocean can be reduced by including the cloud micro-physics or by the vertical mixing of ocean temperatures in that region. These possibilities could also be explored in PlaSim in the future but have not yet been implemented.

In light of the analysis presented, the choice of the PlaSim-LSG T21 configuration seems to be a reasonable and justified one for the purpose of this study. While the model does exhibit notable biases, especially in the Southern Hemisphere, these limitations do not critically impact the investigation of the phenomena of interest, which are mainly located in the North Atlantic region. The relatively coarse T21 resolution is sufficient to capture the large-scale dynamics relevant for this study. Overall, PlaSim-LSG provides a good compromise between computational efficiency and a decent description of a coupled atmosphere-ocean system, which altogether shows a good agreement with observations in the region of interest, making it an effective tool to deal with the research questions posed in my master's thesis.

References

[1] Angeloni, M., 2022, "Climate variability in an Earth system Model of Intermediate Complexity: from interannual to centennial timescales," Ph.D. thesis, alma, https://amsdottorato.unibo.it/id/eprint/10152/

[2] Claussen, M., Mysak, L., Weaver, A., Crucifix, M., Fichefet, T., Loutre, M.-F., Weber, S., Alcamo, J., Alexeev, V., Berger, A., et al., 2002, "Earth system models of intermediate complexity: closing the gap in the spectrum of climate system models," Climate dynamics, **18**, pp. 579–586.

[3] Lunkeit, F., Borth, H., Böttinger, M., Fraedrich, K., Jansen, H., Kirk, E., Kleidon, A., Luksch, U., Paiewonsky, P., Schubert, S., Sielmann, F., and Wan, H., 2011, "Planet Simulator Reference Manual Version 16," Meteorologisches Institut, University of Hamburg, https://www.mi.uni-hamburg.de/en/arbeitsgruppen/theoretische-meteorologie/modelle/sources/psreferencemanual-1.pdf

[4] Fraedrich, K., 2012, "A suite of user-friendly global climate models: Hysteresis experiments," The European Physical Journal Plus, **127**(5), p. 53.

[5] Micheels, A. and Montenari, M., 2008, "A snowball Earth versus a slushball Earth: Results from Neoproterozoic climate modeling sensitivity experiments," Geosphere, **4**(2), pp. 401–410.

[6] Roscher, M., Stordal, F., and Svensen, H., 2011, "The effect of global warming and global cooling on the distribution of the latest Permian climate zones," Palaeogeography, Palaeoclimatology, Palaeoecology, **309**(3-4), pp. 186–200.

[7] Hertwig, E., Lunkeit, F., and Fraedrich, K., 2015, "Low-frequency climate variability of an aquaplanet," Theoretical and Applied Climatology, **121**, pp. 459–478.

[8] Fraedrich, K. and Lunkeit, F., 2008, "Diagnosing the entropy budget of a climate model," Tellus A: Dynamic Meteorology and Oceanography, **60**(5), pp. 921–931.

[9] Kilic, C., Raible, C., and Stocker, T., 2017, "Multiple climate states of habitable exoplanets: The role of obliquity and irradiance," The Astrophysical Journal, **844**(2), p. 147.

[10] Fraedrich, K., Kirk, E., and Lunkeit, F., 1998, "Portable university model of the atmosphere," DKRZ Rep, **16**.

[11] Orszag, S. A., 1970, "Transform method for the calculation of vector-coupled sums: Application to the spectral form of the vorticity equation," Journal of Atmospheric Sciences, **27**(6), pp. 890–895.

[12] Eliasen, E., Machenhauer, B., and Rasmussen, E., 1970, "On a numerical method for integration of the hydrodynamical equations with a spectral representation of the horizontal fields," .

[13] Hoskins, B. and Simmons, A., 1975, "A multi-layer spectral model and the semi-implicit method," Quarterly Journal of the Royal Meteorological Society, **101**(429), pp. 637–655.

[14] Simmons, A. J., Hoskins, B. J., and Burridge, D. M., 1978, "Stability of the semi-implicit method of time integration," Monthly Weather Review, **106**(3), pp. 405–412.

[15] Asselin, R., 1972, "Frequency filter for time integrations," Monthly Weather Review, **100**(6), pp. 487–490.

[16] Robert, A., 1981, "A stable numerical integration scheme for the primitive meteorological equations," Atmosphere-Ocean, **19**(1), pp. 35–46.

[17] Fraedrich, K. F., Jansen, H., Kirk, E., Luksch, U., and Lunkeit, F., 2005, "The Planet Simulator: Towards a user friendly model," Meteorologische Zeitschrift, **14**(3), pp. 299–304.

[18] Louis, J.-F., 1979, "A parametric model of vertical eddy fluxes in the atmosphere," Boundary-Layer Meteorology, **17**(2), pp. 187–202.

[19] Roeckner, E., Arpe, K., Bengtsson, L., and Brinkop, S. e. a., 1992, "Simulation of the present-day climate with the ECHAM model: Impact of model physics and resolution," .

[20] Lacis, A. A. and Hansen, J., 1974, "A parameterization for the absorption of solar radiation in the earth's atmosphere," Journal of Atmospheric Sciences, **31**(1), pp. 118–133.

[21] Sasamori, T., 1968, "The radiative cooling calculation for application to general circulation experiments," Journal of Applied Meteorology (1962-1982), pp. 721–729.

[22] Stephens, G. L., Ackerman, S., and Smith, E. A., 1984, "A shortwave parameterization revised to improve cloud absorption," Journal of Atmospheric Sciences, **41**(4), pp. 687–690.

[23] Kuo, H.-L., 1965, "On formation and intensification of tropical cyclones through latent heat release by cumulus convection," Journal of Atmospheric Sciences, **22**(1), pp. 40–63.

[24] Kuo, H.-L., 1974, "Further studies of the parameterization of the influence of cumulus convection on large-scale flow," Journal of Atmospheric Sciences, **31**(5), pp. 1232–1240.

[25] Slingo, A. and Slingo, J. M., 1991, "Response of the National Center for Atmospheric Research Community Climate Model to improvements in the representation of clouds," Journal of Geophysical Research: Atmospheres, **96**(D8), pp. 15341–15357.

[26] Sausen, R., Schubert, S., and Dümenil, L., 1994, "A model of river runoff for use in coupled atmosphere-ocean models," Journal of Hydrology, **155**(3-4), pp. 337–352.

[27] Maier-Reimer, E., Mikolajewicz, U., and Hasselmann, K., 1993, "Mean circulation of the Hamburg LSG OGCM and its sensitivity to the thermohaline surface forcing," Journal of Physical Oceanography, **23**, pp. 731–757.

[28] Drijfhout, S. S., Maier-Reimer, E., and Mikolajewicz, U., 1996, "Tracing the conveyor belt in the Hamburg large-scale geostrophic ocean general circulation model," Journal of Geophysical Research: Oceans, **101**(C10), pp. 22563–22575.

[29] Hasselmann, K., 1982, "An ocean model for climate variability studies," Progress in Oceanography, **11**(2), pp. 69–92.

[30] Bryan, K. and Lewis, L., 1979, "A water mass model of the world ocean," Journal of Geophysical Research: Oceans, **84**(C5), pp. 2503–2517.

[31] Arakawa, A. and Lamb, V. R., 1977, "Computational design of the basic dynamical processes of the UCLA general circulation model," .

[32] Lorenz, S., 2006, "Coupling of Planet Simulator (atmosphere) with Large Scale Geostrophic (ocean) general circulation model: PlaSim/LSG," Theoretische Meteorologie, University of Hamburg.

[33] Mehling, O., Bellomo, K., Angeloni, M., Pasquero, C., and von Hardenberg, J., 2023, "High-Latitude Precipitation as a Driver of Multicentennial Variability of the AMOC in a Climate Model of Intermediate Complexity," Climate Dynamics, **61**(3), pp. 1519–1534.

[34] Angeloni, M., Palazzi, E., and Hardenberg, J., 2020, "Evaluation and climate sensitivity of the PlaSim v.17 Earth System Model coupled with ocean model components of different complexity," .

[35] Lan, X., Tans, P., and Thoning, K., 2025, "Trends in globally-averaged CO2 determined from NOAA Global Monitoring Laboratory measurements," NOAA Global Monitoring Laboratory.

[36] Ramaswamy, V., Boucher, O., Haigh, J., Hauglustaine, D., Haywood, J., Myhre, G., Nakajima, T., Shi, G., and Solomon, S., 2001, "Radiative Forcing of Climate Change," Intergovernmental Panel on Climate Change (IPCC), https://www.ipcc.ch/site/assets/uploads/2018/03/TAR-06.pdf

[37] Myhre, G., Highwood, E. J., Shine, K. P., and Stordal, F., 1998, "New estimates of radiative forcing due to well mixed greenhouse gases," Geophysical research letters, **25**(14), pp. 2715–2718.

[38] Buckley, M. W. and Marshall, J., 2016, "Observations, inferences, and mechanisms of the Atlantic Meridional Overturning Circulation: A review," Reviews of Geophysics, **54**(1), pp. 5–63.

[39] Cini, M., Zappa, G., Ragone, F., and Corti, S., 2024, "Simulating AMOC tipping driven by internal climate variability with a rare event algorithm," npj Climate and Atmospheric Science, **7**(1), p. 31.

[40] Ragone, F., Wouters, J., and Bouchet, F., 2018, "Computation of extreme heat waves in climate models using a large deviation algorithm," Proceedings of the National Academy of Sciences, **115**(1), pp. 24–29.

[41] Kahn, H. and Harris, T. E., 1951, "Estimation of particle transmission by random sampling," National Bureau of Standards applied mathematics series, **12**, pp. 27–30.

[42] Moral, P., 2004, *Feynman-Kac formulae: genealogical and interacting particle systems with applications*, Springer.

[43] Giardina, C., Kurchan, J., and Peliti, L., 2006, "Direct evaluation of large-deviation functions," Physical review letters, **96**(12), p. 120603.

[44] Giardina, C., Kurchan, J., Lecomte, V., and Tailleur, J., 2011, "Simulating rare events in dynamical processes," Journal of statistical physics, **145**, pp. 787–811.

[45] Wouters, J. and Bouchet, F., 2016, "Rare event computation in deterministic chaotic systems using genealogical particle analysis," Journal of Physics A: Mathematical and Theoretical, **49**(37), p. 374002.

[46] Flato, G. M., 2011, "Earth system models: an overview," Wiley Interdisciplinary Reviews: Climate Change, **2**(6), pp. 783–800.

[47] Frajka-Williams, E. e. a., 2019, "Atlantic meridional overturning circulation: Observed transport and variability," Frontiers in Marine Science, **6**, p. 260.

[48] Frajka-Williams, E., Foukal, N., and Danabasoglu, G., 2023, "Should AMOC observations continue: how and why?" Philosophical Transactions of the Royal Society A: Mathematical, Physical and Engineering Sciences, **381**(2262), p. 20220195.

[49] Maier-Reimer, E. and Mikolajewicz, U., 1991, "The Hamburg large scale geostrophic ocean general circulation model (cycle 1)," .

[50] Laursen, L. and Eliasen, E., 1989, "On the effects of the damping mechanisms in an atmospheric general circulation model," Tellus A: Dynamic Meteorology and Oceanography, **41**(5), pp. 385–400.

List of Figures

List of Tables